

Layer-resolved shifts of photoemission and Auger spectra from physisorbed rare-gas multilayers

T.-C. Chiang

*Department of Physics and Materials Research Laboratory,
University of Illinois at Urbana-Champaign, Urbana, Illinois 61801*

G. Kaindl and T. Mandel

Institut für Atom- und Festkörperphysik, Freie Universität Berlin, D-1000 Berlin 33, Germany

(Received 11 September 1985)

Rare-gas multilayers adsorbed on Pd(111), Pd(001), and Al(111) were studied with photoemission and Auger spectroscopy. The Xe $4d$ core levels and the Xe $N_{4,5}O_{2,3}O_{2,3}$ Auger transitions show layer-resolved shifts for Xe multilayers on these three substrates. A simple model explains the experimental results satisfactorily. The core-level binding-energy shifts relative to the gas phase are dominated by the final-state hole-screening effect. The Auger kinetic-energy shifts relative to the gas phase, dominated by the difference in initial- and final-state hole-screening energies, are about minus three times the corresponding core-level shifts. The screening energies were calculated using a jellium model for the substrate and a dielectric continuum model for the rare-gas adlayer. Surface-induced shifts of core-level binding energies and Auger kinetic energies for bulk solid Xe(111) were also observed; the theoretical shifts are in very good agreement with the experimental values. The valence levels for multilayers of Ar, Kr, and Xe on Pd(001) were studied. They showed qualitatively similar shifts as the core levels, but the results cannot be explained accurately by our model, because the valence excitations are not as localized as the core excitations. Using spacer layers of Kr and Xe with various thicknesses, the effect of metallic substrate screening on the valence-level shifts of Ar was demonstrated. The issues related to a proper energy-reference level and the question of ionic versus neutral excited states will be discussed.

I. INTRODUCTION

Rare-gas layers adsorbed on metal substrates constitute simple model systems for studies of adsorbate properties and behaviors. The interatomic interactions within the adlayer and between the substrate and the adlayer are relatively weak; thus the experimental results are usually simple, and a clear understanding of the observed phenomena and associated effects is often possible within the framework of some simple models. Photoemission is a particularly powerful technique for studying these systems because it can be performed with a high surface sensitivity and a high resolution to yield direct information about the electronic properties. There have been a number of photoemission studies in the past.¹⁻¹³ Kaindl *et al.* previously reported the observation of layer-resolved core-level and Auger energy shifts for rare-gas multilayers adsorbed on Pd(001).¹ The shifts were explained in terms of differences in screening energies of the core holes, and a very good agreement between experiment and theory was found. Since different atomic layers can be distinguished by the core-level and Auger shifts, processes involving atomic movements can be studied in favorable cases. Kaindl *et al.* demonstrated this technique in a study of thermally induced inversion of a Kr/Xe bilayer on Pd.² Chiang *et al.* also reported the coverage-dependent changes in the work function and core-level binding energies in the submonolayer-coverage regime, and they were able to deduce information about the spatial distribution

of the adatoms.³ Recently, the surface-induced Auger and core-level energy shifts were reported for bulk single-crystal Xe(111).⁴ All these results can be explained quite satisfactorily in terms of differences in hole-screening energies.⁵ Other important photoemission results reported in the literature include the measurement of two-dimensional band dispersions for adsorbed rare-gas monolayers,⁷ and the observation of layer-resolved two-dimensional band dispersions for adsorbed multilayers of Xe on Al(111).⁸

Though some previous publications¹⁻⁵ co-authored by the present authors provided clear evidence for the existence and importance of the hole-screening effect on the core-level and Auger energy shifts, there have been alternative interpretations proposed by the other researchers. For example, Jacobi *et al.* interpreted their data for the shifts of rare-gas valence levels in a number of systems by using an ansatz which ignored the final-state screening effect completely.¹⁰ Opila *et al.* also raised questions concerning the proper reference levels for the binding energies; that is, the location of the adsorbate-induced dipole layer relative to the photoionized adatom.¹¹ Therefore, the interpretation of the data has remained somewhat controversial.

The purpose of the present paper is to discuss in greater detail the layer-resolved core-level, valence-level, and Auger shifts for adsorbed rare-gas films, and new data will be presented. The systems to be discussed include rare-gas layers made of Ar, Kr, and Xe films on three dif-

ferent substrates: Pd(111), Pd(001), and Al(111). A simple model will be used to explain the observed core-level and Auger energy shifts, in which the metallic substrate is replaced by jellium and the Xe adlayer is replaced by a dielectric continuum. The present model is an improved version of the one previously proposed,¹ and involves no arbitrary fitting parameters. By virtue of the good agreement between theory and experiment, we show that the dominant effect leading to the shifts is indeed the hole-screening effect. We will discuss the approximations involved in this model and its range of validity, and show that the shifts in valence-level energies cannot be calculated accurately within this model by nature of the rather spatially extended wave functions associated with the valence levels. The problems and/or controversies mentioned above will be discussed.

The organization of this paper is as follows. A description of the experimental details will be given in Sec. II. Our new data on core-level and Auger energy shifts for Xe films adsorbed on Pd(111) will be presented in Sec. III, which will be followed by Sec. IV on the theoretical model and a comparison between theory and experiment. Similar results on Xe films adsorbed on Pd(001) and Al(111) will be presented in Sec. V. Section VI will focus on the results of valence-level shifts for Ar, Kr, and Xe films adsorbed on Pd(001). A qualitative discussion will be given about the proper interpretation of the shifts. The results for Ar adsorbed on Kr- and Xe-covered Pd(001) will be presented in Sec. VII as a further demonstration of the screening-induced shifts. In Sec. VIII we will discuss some questions of current interest. Section IX concludes the paper.

II. EXPERIMENTAL

The experiments were performed at the Synchrotron Radiation Center of the University of Wisconsin—Madison at Stoughton, Wisconsin. A 3-m toroidal-grating monochromator¹⁴ was used to select the wavelength of synchrotron radiation from the 240-MeV electron storage ring Tantalus. The photoemitted electrons were analyzed with a double-pass cylindrical-mirror analyzer operated with a pass energy of 15 eV in the angle-integrating mode. The substrate-surface normal was pointing into one azimuth of the analyzer acceptance cone; therefore, a significant fraction of the photoemission signal was derived from electrons emitted about the substrate surface normal. The overall instrument resolution for photoemission was typically about 0.2–0.4 eV.

The substrate [Pd(111), Pd(001), or Al(111)] was supported by tungsten wires mechanically anchored to the cold tip of a closed-cycle helium refrigerator. The sample assembly was electrically isolated from the cold tip by a thin sapphire wafer sandwiched between copper plates; therefore, the sample could be independently biased electrically to compensate for the contact-potential difference between the sample and the analyzer. This was important for determining the work function obtained by subtracting the photoemission-spectrum bandwidth from the photon energy. The binding-energy and kinetic-energy scales of the spectra to be presented are all referred to the vacuum level.

The base temperature of the substrate was about 40 K. By passing a current through the supporting tungsten wires, the temperature of the sample could be raised to over 1000 K. The sample temperature was measured with a thermocouple in mechanical contact with the substrate. The substrates were cleaned by repeated sputtering with Ar or Ne ions followed by high-temperature annealing in the usual manner.

High-purity rare gases were used for adsorption on the substrates. In the case of Ar, the gas was further purified by a liquid-nitrogen cold trap. No impurities could be detected on the substrates by photoemission. Under our experimental conditions, the rare-gas layers form (111) hexagonal atomic planes of the fcc lattice. The amount of gas exposure corresponding to a monolayer coverage could be determined to within $\pm 5\%$ by observing in photoemission, as a function of increasing coverage, the development of signals from atoms in the second layer, because photoelectrons from different atomic layers can be distinguished by their different energies. With the exposure calibrated in terms of monolayer coverage, Xe multilayers thicker than the bilayer were prepared by predetermined exposures, as the absolute coverage was linearly proportional to exposure under our experimental conditions. Close-packed monolayers of Ar, Kr, and Xe were formed by depositing slightly thicker layers and then by annealing at a temperature just slightly above the second-layer desorption temperature. Xe bilayers were formed by the same method. Ar and Kr submonolayers adsorbed on top of Xe-covered substrates were prepared by predetermined exposures. All samples were quite stable at the base temperature—the desorption and intermixing rates were so low that no changes in coverage and sample configuration could be detected during the experiment.

To determine the surface Auger and core-level energy shifts for bulk single-crystal Xe(111), we prepared a sample consisting of about 16 layers of Xe on Pd(111). Since the photoelectron escape depth is rather short ($\cong 5$ Å) and the substrate-induced shifts are damped out at large distances, this sample is essentially indistinguishable from bulk single-crystal Xe(111) for our purpose. Films with larger thicknesses tend to charge up appreciably and, therefore, are not suitable for this type of measurement.

III. CORE-LEVEL AND AUGER SHIFTS FOR Xe/Pd(111)

A. Xe 4*d* core levels

Figure 1 shows photoemission spectra (dots) of Xe 4*d* core levels taken with a photon energy $h\nu=90$ eV for (a) a monolayer, (b) a bilayer, (c) a trilayer, and (d) about 16 layers of Xe on Pd(111). The binding energies are referred to the vacuum level of the adsorbate-covered substrate. The spectrum for the monolayer, Fig. 1(a), consists of two peaks corresponding to the spin-orbit-split Xe 4*d*_{3/2} and 4*d*_{5/2} core levels. The spectrum for the bilayer in Fig. 1(b) consists of two sets of subspectra, each resembling the monolayer spectrum. By increasing the Xe coverage gradually from monolayer to bilayer (data not shown here), one can clearly identify the higher-binding-energy set to

be derived from the Xe atoms in the second (top) layer. The intensity for the first layer is less than that for the second layer in Fig. 1(b), because the photoemission signal from the first layer is attenuated by the second layer. Notice that the Xe 4*d* peaks associated with the monolayer are only slightly shifted in energy after the coverage of the second layer. By following the coverage dependence of the line shapes, it is clear that the spectrum for the trilayer in Fig. 1(c) consists of the bilayer spectrum, attenuated by the third layer and very slightly shifted relative to Fig. 1(b), and the contribution from the third layer shifted to higher binding energies. The contributions from the second and third layers are not resolved because

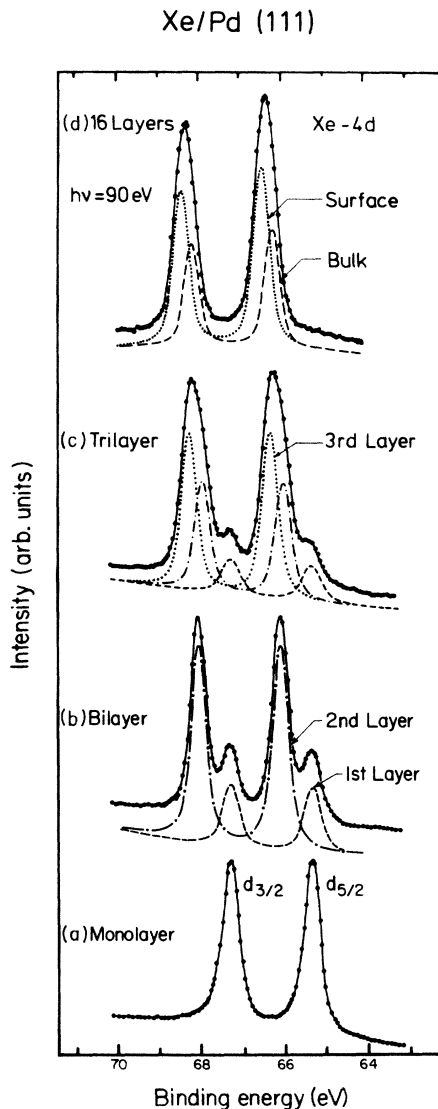


FIG. 1. Xe 4*d* core-level photoemission spectra (dots) for (a) a monolayer, (b) a bilayer, (c) a trilayer, and (d) about 16 layers of Xe on Pd(111). The binding energies are referred to the vacuum level of the adsorbate-covered substrate. The solid curves are the results of a least-squares fit. The decomposition of the spectra into individual layer contributions for the bilayer and trilayer and the decomposition into the surface and bulk contributions for the 16-layer film are indicated.

the relative shift is small; as a result, they combine to form broad and asymmetric peaks as seen in Fig. 1(c). The spectrum for 16 layers of Xe in Fig. 1(d) consists of contributions from all different layers with relative intensities determined by the electron escape depth; therefore, the peaks are measurably broader than those in the monolayer spectrum in Fig. 1(a).

We have analyzed the spectra to obtain the peak positions for different layers. A least-squares-fitting routine was used, and a smooth polynomial background was assumed in each case. Figure 1(a) was fitted first using the convolution of a Doniach-Sunjić (DS) line shape¹⁵ with a Gaussian for each peak. The DS line shape accounts for lifetime broadening and coupling to the conduction electrons in the substrate; the Gaussian line shape accounts for instrumental resolution and possibly inhomogeneous broadening of the observed peaks. The fitting parameters were the width and asymmetry parameter of the DS line shape, the width of the Gaussian line shape, the spin-orbit splitting, the intensities of the two spin-orbit-split components, and the energy position of the $d_{5/2}$ component. The result of the fit is shown in Fig. 1(a) as the solid curve; clearly, the quality of the fit is excellent.

The bilayer spectrum in Fig. 1(b) was fitted by assuming the presence of two sets of spin-orbit-split doublets corresponding to the two layers. The Gaussian width, the spin-orbit splitting, and the DS line-shape asymmetry parameter were assumed to be the same as those for the monolayer. The result of the fit, the solid curve in Fig. 1(b), is also very good. The contributions from the first and second layers are indicated by the dashed and dashed-dotted curves, respectively.

The spectrum for the trilayer shown in Fig. 1(c) and the spectrum for about four layers of Xe (data not shown here) were also analyzed in a similar way. The important numbers from the fit for 1–4 layers of Xe on Pd(111), including the $4d_{5/2}$ binding energies E_B , line-shape parameters W_G , W_D , and A , intensity ratios $I(n, 1)$ between the n th layer and the first layer, and the branching ratio (intensity ratio) between the $d_{5/2}$ and $d_{3/2}$ components, $I(\frac{5}{2}, \frac{3}{2})$, are listed in Table I. The parameters W_G and W_D are the full widths of the Gaussian and DS line shapes, f_G and f_D , respectively. Here,

$$f_G(x) \propto \exp[-4(\ln 2)x^2/W_G^2] \quad (1)$$

and

$$f_D(x) \propto \cos\{\pi A/2 + (1-A)\arctan^{-1}[x/(W_D/2)]\} \\ \times [x^2 + (W_D/2)^2]^{-(1-A)/2}, \quad (2)$$

where A is the asymmetry parameter ($A=0$ corresponds to a Lorentzian line shape). For all four layer configurations, we use $A=0.05$ from the fit to the monolayer spectrum; therefore, the lines are very close to symmetric Lorentzians. In fact, the monolayer spectrum can be fitted very well with A assumed to be zero; the quality of the fit is just slightly worse than that with $A=0.05$ and the difference cannot be easily detected by eye.

In principle, individual atomic layers in the bilayer, trilayer, or quadrilayer may have different line shapes due to differences in environments; therefore, for example, the

TABLE I. Fitting parameters for Xe 4*d* core levels in 1–4 layers of Xe on Pd(111). E_B is the 4*d*_{5/2} binding energy referred to the vacuum level of the adsorbate covered substrate. W_D and W_G are the full widths of Doniach-Šunjić and Gaussian line shapes, respectively. A is the asymmetry parameter. $I(n, 1)$ is the intensity ratio between the n th layer and the first layer. $I(\frac{5}{2}, \frac{3}{2})$ is the branching ratio. All energies are in eV.

Xe/Pd(111)	Monolayer	Bilayer	Trilayer	Four layers
E_B (first layer)	65.33	65.30	65.29	66.24
E_B (second layer)		66.07	65.97	65.86
E_B (third layer)			66.29	66.13
E_B (fourth layer)				66.35
W_D (first layer)	0.28	0.32	0.42	0.24
W_D (second layer)		0.26	0.28	0.24
W_D (third layer)			0.28	0.24
W_D (fourth layer)				0.24
A	0.05	0.05	0.05	0.05
W_G	0.32	0.32	0.32	0.32
$I(2, 1)$		2.68	2.50	2.94
$I(3, 1)$			3.53	7.15
$I(4, 1)$				8.60
$I(\frac{5}{2}, \frac{3}{2})$	1.03	1.13	1.14	1.13

asymmetry parameters and linewidths may be different for different layers because the strength of coupling to the metallic substrate may change. Similarly, the branching ratio generally depends on the final states available for excitation, the matrix elements, and the photoelectron escape probabilities; all these may depend somewhat on the atomic configuration and the location of the layer in the adsorbed film. Theoretically, we should allow all these parameters to vary independently for individual layers in our fitting procedure for maximum accuracy. In practice, however, it is impossible to get a unique fit to a spectrum consisting of unresolved lines if too many degrees of freedom are allowed. Therefore, we have eliminated some degrees of freedom from the fitting procedure; for example, we assume that all atomic layers in the four-layer film have the same DS linewidths, etc. The relative shifts between peaks deduced from the fit, which are the main concern of this paper, did not change appreciably when we tried different but still reasonable assumptions in the fitting procedure. Thus, the fit produces quite accurate values for the relative shifts between peaks, but there may be some errors in the line-shape parameters. The same general comment applies to the analyses of other data to be presented below. The resulting benefit from eliminating unessential degrees of freedom is a tremendous reduction in the time required for computer analysis.

The spectrum for 16 layers of Xe on Pd(111) in Fig. 1(d) consists of unresolved contributions from all layers weighted by the electron escape depth, with about 85% of the intensity coming from the top two layers. Since these contributions are not resolved, a unique fit cannot be obtained by assuming too many free parameters. Following the usual convention in analyzing surface core-level shifts, we assume that there are just two contributions, one from

the surface layer and the other from the bulk, namely all subsurface layers weighted by the escape depth. Furthermore, we assume that the two contributions can be described by Lorentzians convoluted by the same Gaussian function. The DS line shape is not used in this case because the coupling to the metal substrate must be negligible. We started by fitting the monolayer spectrum using a Lorentzian convoluted by a Gaussian. The line-shape parameters obtained were then used as the starting fitting parameters for the two contributions in the 16-layer spectrum. The results of the final fit are shown in Fig. 1(d) and Table II. The quantity of major concern here is the surface core-level shift relative to the bulk. It is 0.26 eV from the fit, which should not depend critically on the above-mentioned assumptions. From our model to be presented below, the bulk contribution, as defined here, should be slightly asymmetrically broadened due to the

TABLE II. Fitting parameters for Xe 4*d* core levels in 16 layers of Xe on Pd(111). W_L is the Lorentzian full width at half maximum, and $I(S, B)$ is the intensity ratio between the surface and the bulk contributions. E_B , W_G , and $I(\frac{5}{2}, \frac{3}{2})$ are as defined in Table I. All energies are in eV.

Xe/Pd(111)	16 layers
E_B (bulk)	66.20
E_B (surface)	66.46
W_L (bulk)	0.18
W_L (surface)	0.22
W_G	0.35
$I(S, B)$	1.64
$I(\frac{5}{2}, \frac{3}{2})$	1.20

presence of many small subsurface shifts, but this is a very small effect, and cannot be deduced from our data easily with finite signal-to-noise ratios.

The photoelectron escape depth λ can be estimated from $I(S,B)$, the intensity ratio between the surface and bulk contributions, by assuming a simple exponential attenuation of the photoemission signal. We have $I(S,B) = \exp(d/\lambda) - 1$, where $d = 3.54 \text{ \AA}$ is the atomic interplanar spacing of Xe(111). This gives $\lambda = 3.65 \text{ \AA}$ for bulk solid Xe(111) at $h\nu = 90 \text{ eV}$.

B. Xe NOO Auger transitions

The Xe $N_{4,5}O_{2,3}O_{2,3}$ Auger transitions were studied for the same layer configurations as described above. Much larger layer-resolved shifts than those for the core levels were observed. In fact, the Auger shifts are about minus three times the corresponding core-level shifts. The spectra (dots) are shown in Fig. 2 together with the results of least-squares fits (solid curves). The fits were done in a fashion similar to those described above for the core levels. The monolayer spectrum in Fig. 2(a) consists of many peaks corresponding to different multiplets, which is very similar to a broadened gas-phase spectrum.¹⁶ To reduce the computation time, we used an asymmetric Lorentzian line shape to simulate the DS line shape for each multiplet component. Again, the quantities of major concern here, the relative shifts in kinetic energy, do not depend appreciably on this approximation. The asymmetric Lorentzian line shape $f_A(x)$ is defined by

$$f_A(x) = (W_A/2)^2 / [x^2 + (W_A/2)^2] \quad (3a)$$

for $x < 0$, and by

$$f_A(x) = (SW_A/2)^2 / [x^2 + (SW_A/2)^2] \quad (3b)$$

for $x > 0$, where S is the line-shape parameter related to the skewness and W_A is related to the width. Convolution with a Gaussian was found to be unnecessary, because the individual components are very wide. The

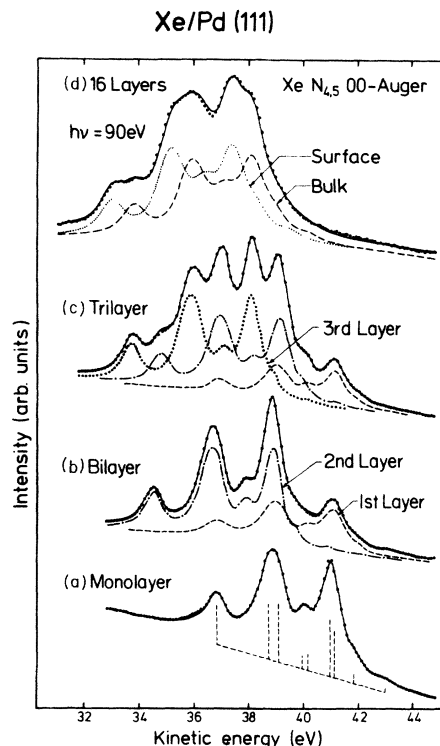


FIG. 2. Xe $N_{4,5}O_{2,3}O_{2,3}$ Auger spectra (dots) of the same four Xe/Pd(111) configurations as in Fig. 1. The kinetic energies are referred to the vacuum level of the adsorbate-covered substrate. The solid curves are the results of a least-squares fit. The bar diagram in (a) shows the relative intensities and positions of different multiplets. The decomposition into individual layer contributions for the bilayer and trilayer and the decomposition into the surface and bulk contributions for the 16-layer film are indicated.

decomposition of the monolayer spectrum into multiplet contributions is indicated in Fig. 2(a) by a bar diagram. The relative positions of the multiplets are in good agreement with the gas-phase data.¹⁶ For simplicity, the

TABLE III. Fitting parameters for Xe NOO Auger transitions in 1–4 layers of Xe on Pd(111). E_K is the kinetic energy for the 1S_0 singlet transition referred to the vacuum level of the adsorbate-covered substrate. W_A is the linewidth. S is the skewness parameter. $I(n,1)$ is the intensity ratio between the n th layer and the first layer. All energies are in eV.

Xe/Pd(111)	Monolayer	Bilayer	Trilayer	Four layers
E_K (first layer)	36.83	36.94	36.96	36.97
E_K (second layer)		34.58	34.83	34.95
E_K (third layer)			33.77	34.27
E_K (fourth layer)				33.64
W_A (first layer)	1.00	1.14	0.90	1.00
W_A (second layer)		0.88	0.88	0.80
W_A (third layer)			0.82	0.70
W_A (fourth layer)				0.82
S	0.71	0.71	0.71	0.71
$I(2,1)$		2.37	2.23	2.83
$I(3,1)$			2.77	2.09
$I(4,1)$				5.67

TABLE IV. Fitting parameters for Xe *NOO* Auger transition in 16 layers of Xe on Pd(111). E_K is the kinetic energy of the 1S_0 transition. W_L is the Lorentzian full width. $I(S,B)$ is the intensity ratio between the surface and the bulk contributions. All energies are in eV.

Xe/Pd(111)	16 layers
$E_K(\text{bulk})$	33.79
$E_K(\text{surface})$	32.98
$W_L(\text{bulk})$	0.86
$W_L(\text{surface})$	0.86
$I(S,B)$	1.15

Auger-electron kinetic energies will be given only for the 1S_0 transition (36.83 eV for the monolayer) in this paper. We obtained $S=0.71$ from the fit for the monolayer spectrum, and the same value of S was used in the fit for 2–4 layers of Xe on Pd(111). As can be seen in Fig. 2, the quality of the fit is again very good. The results of the fit are summarized in Table III.

The thick- (16-) layer spectrum in Fig. 2(d) was fitted assuming the presence of a surface and a bulk contribution with the same line shape, each consisting of multiplet transitions that are the same as in the monolayer spectrum. The best fit was obtained by using symmetric Lorentzians ($S=1$) for the multiplets. The results are given in Table IV. Since each multiplet transition is quite broad, broadening of the bulk contribution due to many small subsurface shifts cannot be detected easily (see below) and, therefore, neglecting this effect does not cause any significant error in the deduced surface Auger shift. The estimated Auger-electron escape depth for Xe(111) is 4.62 Å.

Figure 2(c) shows that the three different layer contributions for the trilayer give rise to well-resolved peaks. Similarly, the 16-layer spectrum in Fig. 2(d) clearly shows resolved peaks that can be separately identified as being due to either the surface or the bulk contributions; the two contributions are indicated by the dotted and dashed curves, respectively.

IV. THEORY

A. Layer-dependent core-level shifts

We will consider the core-level binding-energy shift for a Xe atom in the adsorbed film relative to a free Xe atom. To avoid possible confusion due to contact-potential differences between adjacent crystal faces, this free Xe atom used for reference is supposed to be very close to the substrate surface compared with the lateral dimensions of the sample surface, while the actual distance should be much larger than atomic dimensions. For example, this atom could be at about 0.01 mm above the sample surface of lateral dimensions about 1 cm × 1 cm. The vacuum level of the sample surface corresponds to zero electron kinetic energy in the same region. We shall call this region the vacuum in the following.

Suppose a $4d$ electron is removed from a Xe atom in

bulk solid Xe; this atom will become positively charged because it would cost too much energy (about the band-gap energy) to remove a valence electron from a nearby Xe atom and put it onto the ionized atom. Consequently, the final-state screening of a core hole generated by photoionization in solid Xe involves mainly long-range polarization of other Xe atoms. On the other hand, if the Xe atom under consideration is in contact with a metal substrate, it is not immediately obvious if the atom becomes charged or neutral after screening sets in, because it would cost much less energy to transfer an electron from the metal substrate onto the photoionized Xe adatom. Recent experimental and theoretical results indicate that the Xe adatom is nearly fully charged for most substrates.^{3,17,18} We will assume in our model that the Xe adatom in the photoemission or Auger final states is fully charged. The justification relies partly on the good agreement between theory and experiment. We will discuss this point more fully below.

Consider a Xe adatom $Xe(n,m)$ in the n th layer of an m -layer film ($m \geq n$). The $4d$ binding energy of this atom, $E_B(n,m)$, relative to the vacuum level, is defined by

$$E_B(n,m) = h\nu - E_K(n,m), \quad (4)$$

where $h\nu$ is the photon energy and $E_K(n,m)$ is the photoelectron kinetic energy in the vacuum. The *same* final state involving the ionized adatom $Xe^+(n,m)$ can be reached from the *same* initial state by the following hypothetical process. We move the $Xe(n,m)$ atom into the vacuum by providing the cohesive energy $E_c(n,m)$, which is derived from the short-range van der Waals interaction. The atom is then photoionized in the vacuum:

$$E_B(F) = h\nu - E_K(F), \quad (5)$$

where $E_B(F)$ and $E_K(F)$ are the $4d$ binding energy and the photoelectron kinetic energy of the free atom, respectively. Now we move this ionized atom back to its original location in the film, during which process a bonding energy $E_c^+(n,m)$ is released. Applying energy conservation evaluated according to this hypothetical process, the $4d$ binding energy of $Xe(n,m)$ is just the total energy input to the system,

$$E_c(n,m) + h\nu - E_c^+(n,m),$$

subtracting the photoelectron kinetic energy $E_K(F)$; therefore,

$$E_B(n,m) = E_c(n,m) + h\nu - E_c^+(n,m) - E_K(F). \quad (6)$$

Combining Eqs. (5) and (6), we obtain the binding-energy shift of $Xe(n,m)$ relative to a free Xe atom,

$$\Delta E_B(n,m) = E_c(n,m) - E_c^+(n,m), \quad (7)$$

where the binding energies are measured relative to the vacuum level. The first and second terms on the right-hand side of Eq. (7) are quantities pertaining to the initial and final states of the system, respectively, and hence can be identified with the initial- and final-state shifts. Note that the breakdown of ΔE_B into the initial- and final-state shifts may depend on the theoretical model, and is not necessarily unique.

$E_c(n,m)$ is generally small, being 0.17 eV for bulk solid Xe at 0 K.¹⁹ It is even smaller for atoms located at the surface of solid Xe. E_c is somewhat larger if the atom is adsorbed directly on the metal substrate, but even then the heat of adsorption is, e.g., only about 0.3, 0.28, 0.40, and 0.41 eV, respectively, for Xe on Pd(001),²⁰ Ag(111),²¹ W(111),²² and Pd(110).²³ We do not have reliable values for the heat of adsorption for Xe on Pd(111) and Al(111), but they must be approximately 0.2–0.4 eV. Therefore, the initial-state shift is roughly 0.1–0.2 eV for Xe(n,m), with $n > 1$, and 0.2–0.4 eV for Xe(1, m). Lang¹⁷ calculated the initial-state shift for a single Xe adatom on a jellium substrate [with parameters chosen to simulate Al(111)] using a local-density-functional formalism, and obtained a value of about 0.3 eV, in good agreement with our estimate of 0.2–0.4 eV.

The bonding energy $E_c^+(n,m)$ has possibly three major contributions:

$$E_c^+(n,m) = E_s(n,m) + E'_c(n,m) - b(n,m)\Delta W(m). \quad (8)$$

$E_s(n,m)$ is the long-range screening energy due to the positive charge associated with the core hole, which can be accurately described by the classical image formula.¹ $E'_c(n,m)$ is a short-range van der Waals-type energy. The ionized adatom $\text{Xe}^+(n,m)$ polarizes the surrounding atoms, and its own valence orbitals also shrink somewhat compared to an unexcited Xe atom. E'_c would be the bonding energy of $\text{Xe}^+(n,m)$ without the core hole if the polarization configuration induced by the core hole could be held frozen. Since $\text{Xe}^+(n,m)$, as well as unexcited $\text{Xe}(n,m)$, has a closed-valence-shell configuration, E'_c is of the same order as E_c . The third term in Eq. (8) is the negative of the potential energy of the positive ion in the field of the dipole layer on the surface, where $\Delta W(m)$ is the part of the work function corresponding to the dipole layer of the substrate covered by m layers of Xe, and $b(n,m)$ is a positive parameter depending on the position of the core hole relative to the dipole layer.¹¹ $b=0$ if the core hole is outside the dipole layer. Generally, $0 \leq b \leq 1$. For adsorbed rare-gas films on metal substrates, the dipole layer is generally confined spatially between the first rare-gas atomic layer and the substrate surface.^{3,24} Thus, the third term in Eq. (8) can be neglected for $n > 1$; that is, $b(n,m)=0$ for $n > 1$, because the core hole is outside the dipole layer. Similarly, $b(1,m)$ is nearly independent of m . Opila *et al.*,¹¹ using a dipole-summation technique and assuming a certain dipole configuration, showed that $b(1,1) \simeq 0.75$ for core levels of Xe adsorbed on oxygen-covered W(110). However, a quantum-mechanical calculation of Lang *et al.* indicated that $b(1,m) \simeq 0$ for core levels of Xe adsorbed on metals, in agreement with recent experimental results.²⁴ Since the calculation of Lang *et al.* employed a more reliable model and since our system involves metal substrates, we are convinced that the results of Lang *et al.* are applicable in our case. Therefore, we have

$$b(n,m) \simeq 0 \quad (9)$$

for all n and m in the case of Xe core levels; that is, the core hole is outside the dipole layer. From Eqs. (7)–(9) and $E'_c \simeq E_c$, we obtain

$$\Delta E_B(n,m) \simeq -E_s(n,m), \quad (10)$$

indicating that the binding-energy shift is given to a high degree of accuracy by the negative of final-state hole-screening energy.¹

It remains to calculate $E_s(n,m)$. Figure 3 shows schematically the model viewed sideways with the vacuum being above the Xe-covered Pd(111) substrate. The Pd and Xe atomic locations in one cross section are indicated by open and solid circles, respectively. We use the jellium model²⁵ for the Pd substrate; each Pd atomic plane is replaced by a jellium slab of thickness equal to the atomic interplanar spacing. The boundaries of the jellium slabs are indicated by the long-dashed lines in Fig. 3. The upper boundary of the topmost jellium slab is referred to as the positive-background edge. Lattice relaxation is ignored here, which is generally small in most metals. Due to electron spillage, the image plane, indicated by the short-dashed line in Fig. 3, is located at a distance $x_0 = 0.846$ Å above the positive-background edge from a local-density-functional calculation for $r_s = 2$ appropriate for Pd and Al.²⁵ From the same calculation, the screening energy of a point charge e outside the metal is given by the classical image formula $e^2/4z$, where z is the distance between the charge e and the image plane, provided z is sufficiently large. For Xe adsorbed on Pd or Al, this large- z condition is well satisfied, because the Xe atomic radius is relatively large. In our model, screening by the metal substrate is taken to be entirely classical in the sense described above.

The Xe monolayer on Pd or Al is a close-packed hexagonal layer incommensurate with the substrate. The distance between the Xe nucleus and the image plane is taken to be the average distance calculated from a hard-sphere model. The hard sphere associated with a Xe adatom is in contact with the hard spheres associated with the metal surface. The average distance is obtained by sampling equally all possible adatom positions relative to the substrate in a plane parallel to the substrate surface. The hard-sphere radii are taken to be the standard atomic ra-

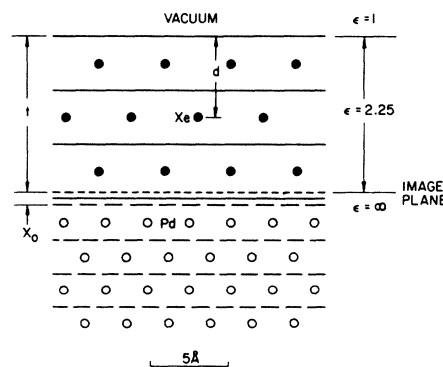


FIG. 3. Theoretical model for a trilayer of Xe on Pd(111). The Xe and Pd atoms are indicated by solid and open circles, respectively. The solid and long-dashed lines indicate the boundaries of the dielectric slabs and the jellium slabs, respectively, for individual atomic layers. The short-dashed line indicates the image plane.

dii. This procedure usually yields results in fairly good agreement (± 0.2 Å) with low-energy electron-diffraction (LEED) results,²⁶ although no LEED results are available for the systems studied here.

For a few or more layers of Xe adsorbed on Pd or Al, the crystal structure is face-centered cubic with the [111] direction along the surface normal. The distance between two adjacent Xe atomic planes is taken to be the same as in bulk solid Xe. Thus, all Xe atomic layer positions are determined relative to the substrate.

We use the dielectric continuum model to describe the polarization response of the adsorbed Xe film to the core hole. Each Xe atomic layer is replaced by a dielectric slab of thickness equal to the atomic interplanar spacing and with a dielectric constant equal to that of bulk solid Xe ($\epsilon=2.25$). The use of a dielectric constant is justified because only the adiabatic limit is considered here. Since we are mainly interested in differences in atomic energies, we can expect that the intra-atomic contributions are largely canceled when differences are taken; therefore, the atomic structure can be neglected to first order, as in the present model. Screening due to the dielectric continuum is taken

to be entirely classical. The boundaries of the dielectric slabs are indicated by solid lines in Fig. 3.

Figure 3 gives, roughly to scale, a schematic of a tri-layer of Xe on Pd(111). The model is summarized on the right-hand side of the figure. The dielectric constant for the space below the image plane associated with metallic Pd(111) is set to be infinite. For the space between the image plane and the upper dielectric boundary $\epsilon=2.25$ is assumed. Note that the lower dielectric boundary would actually be slightly below the image plane in Fig. 3, but we terminate the dielectric at the image plane, since metallic screening ($\epsilon=\infty$) is much more effective than dielectric screening. The distance between an ionized Xe atom and the vacuum-dielectric boundary is denoted by d , as indicated by the example shown in Fig. 3, where a Xe atom in the second layer is under consideration. The distance between the vacuum-dielectric boundary and the image plane is denoted by t (for thickness).

The screening energy for a core hole with charge e (taken to be a point charge) can be easily evaluated by solving the Poisson's equation in the usual manner according to our model. We obtain, using Eq. (10),

$$\Delta E_B(n, m) - \Delta E_B(\infty/2, \infty) = -e^2/[4\epsilon(t-d)] + (e^2/2\epsilon) \sum_{p=1}^{\infty} (-\mu)^p \{ 1/pt - 1/[2(p-1)t+2d] - 1/[2(p+1)t-2d] \}, \quad (11)$$

where $\epsilon=2.25$ is the dielectric constant of a bulk Xe crystal, $\mu=(\epsilon-1)/(\epsilon+1)$, and t and d , defined above, are functions of m and n . Equation (11) has the form of a sum involving an infinite number of image charges. $\Delta E_B(\infty/2, \infty)$ is the core-level binding-energy shift for a Xe atom deep inside bulk solid Xe relative to a free atom, and is the value of $\Delta E_B(n, m)$ in the limits $m \rightarrow \infty$ and $n \rightarrow \infty$ while $0 < n/m < 1$. Equation (11) simply gives the core-level binding-energy shift for Xe(n, m) relative to a Xe atom deep inside bulk solid Xe. To understand Eq. (11), consider a sample in which half of the substrate surface is covered with an m -layer Xe film, while the other half is covered with a thick ($m \rightarrow \infty$) Xe film. Since the work function of the substrate does not change appreciably beyond monolayer coverage, the two halves have the same vacuum reference level, and the core-level binding-energy shifts on the two halves can be compared directly.

Within our dielectric continuum model, we have

$$\Delta E_B(\infty/2, \infty) = \left[\int \epsilon F^2 dv - \int F_0^2 dv \right] / 8\pi, \quad (12)$$

using Eq. (10), where $\epsilon=2.25$, and F and F_0 are the electric fields of the ionized Xe atom inside the solid and in the vacuum, respectively. This is the core-level shift of bulk solid Xe relative to a free Xe atom.²⁷ The volume of integration is over all space, excluding the volume occupied by the Xe ion, since the intra-atomic screening energy does not change in a first-order approximation. With

$$F = e/\epsilon r^2 \quad (13)$$

and

$$F_0 = e/r^2, \quad (14)$$

where r is the polar coordinate, Eq. (12) becomes

$$\Delta E_B(\infty/2, \infty) = -(1-1/\epsilon)e^2/2r_0. \quad (15)$$

r_0 in Eq. (15) is defined such that $4\pi r_0^3/3$, the volume of a sphere with radius r_0 , is equal to $a^3/4$, the volume occupied by a Xe atom in solid Xe, where a is the lattice parameter. We then obtain

$$\Delta E_B(\infty/2, \infty) = -1.66 \text{ eV}. \quad (16)$$

Our value for ΔE_B is slightly different from that obtained by Himpsel *et al.* (-1.84 eV), who used a different criterion to obtain r_0 .²⁷ This uncertainty indicates the order of accuracy of our calculation. The model-dependent factor r_0 enters Eq. (15) because the difference involving two phases, gas and solid, has to be calculated. For a more accurate value of $\Delta E_B(\infty/2, \infty)$, the atomistic structure of bulk solid Xe has to be taken into account. For comparison, Eq. (11) involves the difference only between atoms in the same solid phase and contains no such factors as r_0 ; therefore, the results are expected to be more accurate.

Combining Eqs. (11) and (16), we have calculated the Xe $4d$ binding-energy shifts, $\Delta E_B(n, m)$, with $1 \leq n \leq m \leq 4$ for Xe on Pd(111). The theoretical values, labeled $\Delta E_B(\text{theor. } 1)$, are listed in Table V together with the experimental values $\Delta E_B(\text{expt.})$ derived from Table I. The $4d_{5/2}$ and $4d_{3/2}$ binding energies of gas-phase Xe are taken to be 67.55 and 69.52 eV, respectively.²⁸ Clearly, the theoretical values are generally in good agreement with the experimental values, considering the approximations

TABLE V. Xe $4d$ core-level shifts ΔE_B and Xe NOO Auger-electron kinetic-energy shifts ΔE_K for 1–4 layers and 16 layers of Xe on Pd(111). Three different theoretical values [(theor. 1)–(theor. 3)] for ΔE_B are listed. All energies are in eV. The experimental values of $|\Delta E_K/\Delta E_B|$ are also listed.

Xe/Pd(111)	Layer	ΔE_B (expt.)	ΔE_B (theor. 1)	ΔE_B (theor. 2)	ΔE_B (theor. 3)	ΔE_K (expt.)	$ \Delta E_K/\Delta E_B $ (expt.)
Monolayer	1	-2.22	-2.69	-2.47	-2.20	7.10	3.20
Bilayer	1	-2.25	-2.78	-2.56	-2.31	7.21	3.20
	2	-1.48	-1.77	-1.55	-1.52	4.85	3.27
Trilayer	1	-2.26	-2.78	-2.56	-2.32	7.23	3.20
	2	-1.58	-1.95	-1.73	-1.70	5.10	3.22
	3	-1.26	-1.59	-1.37	-1.36	4.04	3.20
Four layers	1	-2.31	-2.78	-2.56	-2.32	7.06	3.06
	2	-1.69	-1.97	-1.75	-1.72	5.24	3.10
	3	-1.42	-1.80	-1.58	-1.57	4.54	3.20
	4	-1.19	-1.51	-1.29	-1.29	3.91	3.28
Thick film (≈ 16 layers)	bulk	-1.35	-1.57	-1.35	-1.35	4.06	3.01
	surf.	-1.09	-1.31	-1.09	-1.09	3.25	2.98

and uncertainties involved in our model. Most importantly, the general trends of the experimental shifts are reproduced by the theory. The small numerical discrepancies will be discussed below.

B. Surface core-level shifts

The thick film (about 16 layers) of Xe on Pd(111) is indistinguishable from bulk solid Xe for photoemission measurements. Since only the top few layers are probed, setting $m=16$ or ∞ in Eq. (11) makes no practical difference. We obtain from Eq. (11), in the limits of large m and n with finite $m-n$ (that is, $t \rightarrow \infty$, d remains finite in Fig. 3),

$$\Delta E_B(d) - \Delta E_B(\infty/2, \infty) = \mu e^2/4\epsilon d, \quad (17)$$

where we now label ΔE_B in terms of the distance d . This is just the simple image formula for a single dielectric-vacuum boundary.²⁹ The predicted shifts $\Delta E_B(d)$ from

Eqs. (16) and (17) are listed in Table VI for different layers. The relative intensities, calculated using the experimentally determined escape depth, are also shown. Clearly, the relative intensities decrease very rapidly for deeper layers, as do the relative shifts. The bulk contribution as determined from the fit shown in Fig. 1 is essentially the average contribution from all the subsurface layers weighted by the relative intensities. The line shape should be slightly asymmetrically broadened, but this is a very small effect and we do not expect to be able to detect this easily as discussed above. The theoretical value of ΔE_B for the bulk contribution, obtained by calculating the intensity-weighted average of ΔE_B for all subsurface layers, is -1.57 eV (given in Table VI), which is very close to $\Delta E_B(\infty/2, \infty) = -1.66$ eV. For easy comparison, the theoretical and experimental shifts for the bulk and surface contributions are also listed in Table V. The relative shift between the surface and bulk contributions, being $-1.31 - (-1.57) = 0.26$ eV theoretically, is the

TABLE VI. Theoretical layer-resolved $4d$ -core-level shifts ΔE_B and NOO Auger-electron energy shifts ΔE_K for bulk solid Xe(111) relative to the gas phase. Surface layer n means the n th layer below the surface layer. $I(4d)$ and $I(NOO)$ are the relative intensities of the layer contribution to the photoemission and Auger spectra, respectively; the surface layer is assumed to have an intensity equal to 1. The intensity-weighted average values of ΔE_B and ΔE_K for all subsurface layers are also shown. All energies are in eV.

Bulk Xe(111)	ΔE_B (theor.)	$I(4d)$	ΔE_B (theor.)	ΔE_K (theor.)	$I(NOO)$	ΔE_K (theor.)
Surface layer	-1.31	1.000	-1.31	3.94	1.000	3.94
Surface layer 1	-1.54	0.379	Ave.	4.63	0.465	Ave.
Surface layer 2	-1.59	0.144		4.77	0.216	
Surface layer 3	-1.61	0.021		4.83	0.100	
Surface layer 4	-1.62	0.003		4.86	0.047	
⋮	⋮	⋮		⋮	⋮	
Surface layer ∞	-1.66	0.000	-1.57	4.98	0.000	4.72

same as the experimental value, given by $-1.09 - (-1.35) = 0.26$ eV. These values are listed in Table VII. Again, we want to emphasize that our theory is more accurate in predicting the differences involving atoms in the same phase.

C. Causes of difference between theory and experiment

Referring to Table V, the general trends of the core-level shifts are reproduced very well by the theory. Although the theoretical values of $|\Delta E_B|$ are slightly larger than the experimental values in all cases, the differences are at most about 0.5 eV. This is about the accuracy we expect from the approximations made in the theory.

As discussed above, Eq. (15) is relatively inaccurate. Any inaccuracy in $\Delta E_B(\infty/2, \infty)$ is reflected in all the theoretical values in Tables V and VI through Eq. (11). If we use the experimental value for the solid-to-gas shift, $\Delta E_B(\infty/2, \infty)$, this inaccuracy can be removed. This is equivalent to changing the reference from the gas phase to bulk solid Xe. We have not really measured $\Delta E_B(\infty/2, \infty)$. Rather, we have measured ΔE_B for the bulk contribution from a 16-layer film, $\Delta E_B(b, 16)$, but this is very close to $\Delta E_B(\infty/2, \infty)$.

The column in Table V labeled $\Delta E_B(\text{theor. 2})$ gives the adjusted theoretical values of ΔE_B , which are obtained by adding 0.22 eV to $\Delta E_B(\text{theor. 1})$ in Table V. This adjustment simply makes the theoretical value of $\Delta E_B(b, 16)$ equal to the experimental value. In this way, the inaccuracy in $\Delta E_B(\infty/2, \infty)$ is essentially eliminated. The resulting values of $\Delta E_B(\text{theor. 2})$ are in better agreement with experiment; the differences are only about 0.3 eV for the atomic layers in direct contact with the substrate, and much less for the other layers.

In our model theory the remaining small differences can be due to (1) the inaccuracy in locating the first monolayer relative to the substrate (estimated uncertainty about 0.2 Å); (2) the inaccuracy in the position of the image plane relative to the substrate; (3) the differences between E'_c and E_c ; and (4) the $b \Delta W$ term in Eq. (8). The last two reasons are probably less important than the first two. The local density-functional theory has a limited accuracy, and we really should use the dynamic image plane rather than the static image plane in our model. However, we have no better theory at the present time.

The column in Table V labeled $\Delta E_B(\text{theor. 3})$ gives the theoretical shifts further adjusted from $\Delta E_B(\text{theor. 2})$ by moving the image plane downward relative to the Xe layers (or moving the Xe layers upward relative to the Pd substrate; see Fig. 3) by 0.4 Å. The values of $\Delta E_B(\text{theor. 3})$ are very close to the experimental values in all cases. Conceivably, a 0.4-Å adjustment can be explained by reasons mentioned above, but this shall be established in future studies. The remaining small differences of no more than 0.15 eV between $\Delta E_B(\text{theor. 3})$ and the experimental values can be easily accounted for by experimental inaccuracies.

D. Layer-dependent Auger shifts

The derivation for the Auger kinetic-energy shift $\Delta E_K(n, m)$ for an atom in the n th layer of an m -layer film

relative to a free Xe atom is quite analogous to the derivation for the core-level binding-energy shift. Assuming that the final state of the Auger transition is doubly ionized whether the atom is in direct contact with the metal substrate or not, we obtain [see Eq. (7)]

$$\Delta E_K(n, m) = -E_c^+(n, m) + E_c^{++}(n, m), \quad (18)$$

where $E_c^{++}(n, m)$ is the bonding energy of the doubly ionized atom in the final state. The two terms on the right-hand side of Eq. (18) give the initial- and final-state shifts, respectively. As discussed earlier [see Eqs. (8) and (9)],

$$E_c^+(n, m) \simeq E_s(n, m) + E'_c(n, m). \quad (19)$$

Similarly,

$$E_c^{++}(n, m) \simeq 4E_s(n, m) + E_c''(n, m), \quad (20)$$

where $E_c''(n, m)$, analogous to $E'_c(n, m)$, is the short-range part of the bonding energy of the doubly ionized atom. Since the screening energy is proportional to the square of the charge [see Eq. (11)], the screening energy for $\text{Xe}^{++}(n, m)$ is just 4 times that for $\text{Xe}^+(n, m)$. If the atom is not in direct contact with the Pd substrate, E'_c and E_c'' are both small and of the same order as E_c , because the bonding is only with neighboring neutral Xe atoms. We can ignore the difference between E'_c and E_c'' compared with the difference in the screening energies; from Eqs. (18)–(20), we obtain

$$\Delta E_K(n, m) \simeq 3E_s(n, m). \quad (21)$$

Using Eq. (10), we also obtain

$$\Delta E_K(n, m) \simeq -3\Delta E_B(n, m). \quad (22)$$

Thus the Auger kinetic-energy shifts should be about minus three times the corresponding core-level binding-energy shifts. The experimentally measured ΔE_K and the ratio $|\Delta E_K/\Delta E_B|$ are given in Table V for all layer configurations. The ratios are indeed very close to 3 (within less than 10%), even for the layers in direct contact with the metal substrate ($n=1$).

For $n=1$, E_c'' may be larger than E'_c , because the $N_{4,5}O_{2,3}O_{2,3}$ Auger final state has an open $5p$ valence shell. There may be a stronger chemisorption-type bond to the metal substrate in the final state with an energy of the order of that for Te (also having a $5p^4$ configuration) adsorbed on Pd(111). We do not know this energy; besides, the equilibrium adsorption distance between Te and Pd is different from that between Xe and Pd. Since the Auger spectrum for monolayer Xe on Pd(111) has a line shape quite similar to that for the gas phase, the chemisorption bond must be weak, implying a small E_c'' .³⁰ Assuming, for example, that $E_c'' - E'_c = 0.5$ eV, which is not atypical for a weak chemisorption bond, we obtain $|\Delta E_K/\Delta E_B| \simeq 3.2$ using Eqs. (10) and (18)–(20). This is still consistent with our experimental observation. A similar effect may also exist, although to a lesser degree, for $n > 1$.

Since the *NOO* Auger two-hole final state is more spatially extended than the initial state, there may be a non-negligible overlap between the charge distribution and the dipole layer in the final state for $n=1$. This can lead to a

TABLE VII. Experimental and theoretical values for the surface-induced shifts in Auger-electron kinetic energy and core-level binding energy relative to the bulk for solid Xe(111). The ratios of the Auger-to-core shifts are also shown. All energies are in eV.

Bulk Xe(111)	Experiment	Theory
Surface Auger shift	-0.81	-0.78
Surface core shift	0.26	0.26
Ratio	-3.1	-3.0

reduction in $E_c^{++}(1,m)$ [see Eq. (8) and associated discussion], and hence a reduction in $\Delta E_K(1,m)$. Unfortunately, a reliable calculation of this effect does not exist.

Experimentally, Eq. (22) holds very well in all cases. Therefore, the two effects mentioned above are either relatively small or nearly cancel each other. This problem remains to be solved in future studies.

E. Surface Auger shifts

Using Eqs. (17) and (22), we have evaluated the Auger shifts for various layers in a thick film, which are just minus three times the corresponding core-level shifts. The results are listed in Table VI. Also given are the relative intensities of different layers using the experimentally determined escape depth (which is different from the value for the core-level photoelectrons because the kinetic energies are different). Experimentally, the subsurface shifts are not resolved. The average contribution weighted by intensity from all subsurface layers gives the bulk contribution; the corresponding ΔE_K is shown in Table VI. In principle, the bulk contribution should have an asymmetric line shape for each Auger component due to this effect, but this is too small to be determined precisely. We have ignored this effect in our fitting procedure as discussed above.

From Table VI, the theoretical surface Auger shift relative to the bulk is $3.94 - 4.72 = -0.78$ eV, in good agreement with the experimental value of $3.25 - 4.06 = -0.81$ eV (see Table V). These values and the ratios of Auger-to-core shifts are listed in Table VII for comparison.

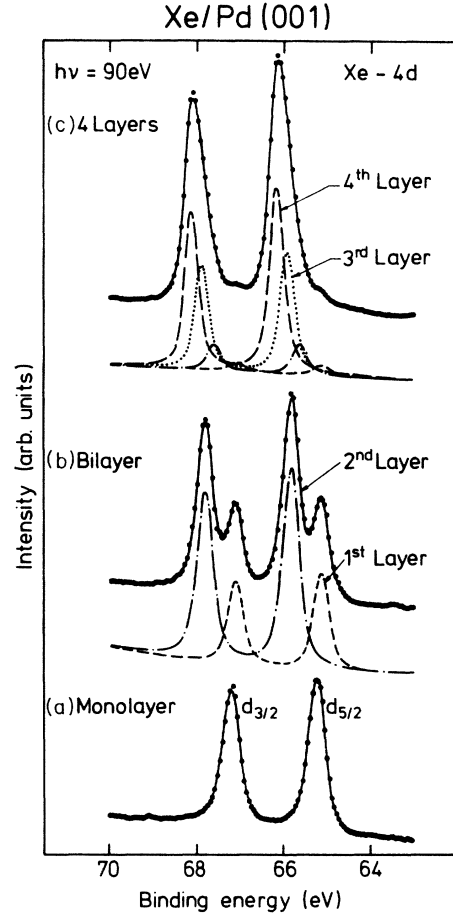


FIG. 4. Xe $4d$ core-level photoemission spectra for (a) a monolayer, (b) a bilayer, and (c) a quadrilayer of Xe on Pd(001). The symbols and notations are similar to those in Fig. 1.

V. CORE-LEVEL AND AUGER SHIFTS FOR Xe/Pd(001) AND Xe/Al(111)

The results for Xe on Pd(001) and Al(111) are very similar to those for Xe on Pd(111) already discussed above. The $4d$ core-level spectra and the NOO Auger spectra for these systems are shown in Figs. 4–7. The re-

TABLE VIII. Xe $4d$ core-level shifts ΔE_B and Xe NOO Auger-electron energy shifts ΔE_K for monolayer, bilayer, and four layers of Xe on Pd(001). All energies are in eV. The experimental values of $|\Delta E_K/\Delta E_B|$ are also listed.

Xe/Pd(001)	Layer	ΔE_B (expt.)	ΔE_B (theor. 1)	ΔE_K (expt.)	$ \Delta E_K/\Delta E_B $ (expt.)
Monolayer	1	-2.32	-2.61	6.77	2.92
Bilayer	1	-2.39	-2.70	6.90	2.89
	2	-1.68	-1.76	4.88	2.90
Four layers	1	-2.47	-2.70	7.05	2.92
	2	-1.89	-1.96	5.42	2.87
	3	-1.62	-1.79	4.84	2.99
	4	-1.38	-1.51	4.09	2.96

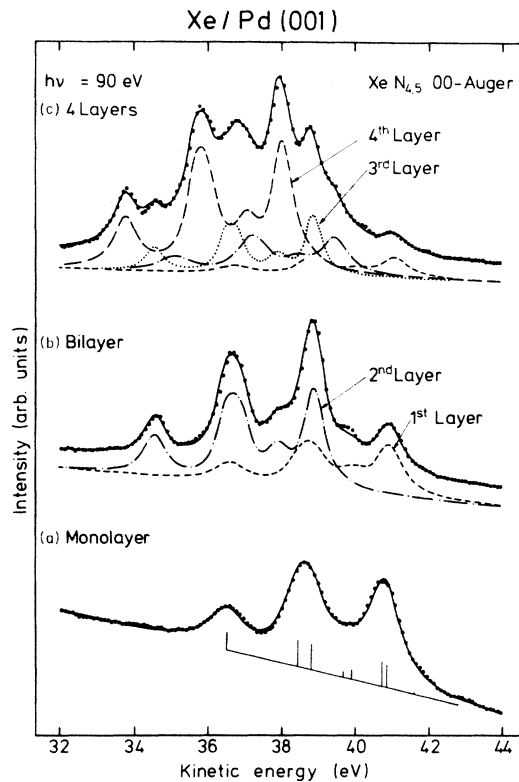


FIG. 5. Xe $N_{4,5}O_{2,3}$ Auger spectra of the same three Xe/Pd(001) configurations as in Fig. 4. The symbols and notations are similar to those in Fig. 2.

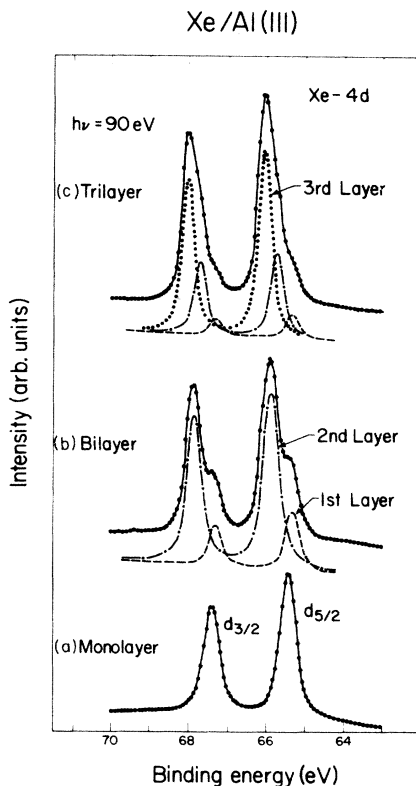


FIG. 6. Xe $4d$ core-level photoemission spectra for (a) a monolayer, (b) a bilayer, and (c) a trilayer of Xe on Al(111). The symbols and notations are similar to those in Fig. 1.

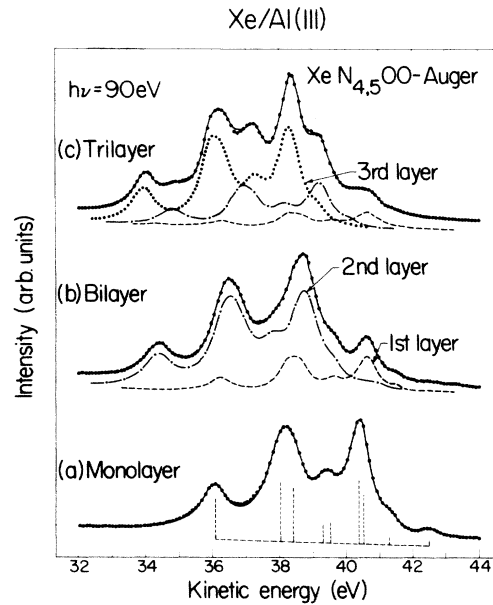


FIG. 7. Xe $N_{4,5}O_{2,3}$ Auger spectra of the same three Xe/Al(111) configurations as in Fig. 6. The symbols and notations are similar to those in Fig. 2.

sults of a least-squares fit are also shown; the notations are similar to those used in Figs. 1 and 2. Clearly, the layer-dependent shifts seen in Xe/Pd(111) are also observed in these systems.

Without going into details, we show the core-level and Auger shifts derived from the least-squares fits in Tables VIII and IX for Xe/Pd(001) and Xe/Al(111), respectively. The magnitudes of the shifts are very close to those found in Xe/Pd(111). Also shown in Tables VIII and IX are the theoretical values of the core-level shifts, $\Delta E_B(\text{theor. } 1)$, without any adjustment. The differences between theoretical and experimental binding-energy shifts follow the same trends as observed in Xe/Pd(111). The maximum difference is about 0.6 eV for Xe/Al(111) and about 0.3 eV for Xe/Pd(001) occurring for the layers in direct contact with the metal substrates. With adjustments of the theoretical values as discussed for Xe/Pd(111), the differences can be reduced to the level of experimental errors. There are no qualitative differences among the three systems studied. In Tables VIII and IX, the ratios $|\Delta E_K/\Delta E_B|$ are also listed, which are again very close to 3 (within 7%); essentially all the ratios are somewhat less than 3, in contrast to the case of Xe/Pd(111), where almost all the ratios are somewhat larger than 3. This difference is likely due to the limited accuracy of the applied theory and also to experimental errors (e.g., the experimental error in determining the vacuum level is estimated to be ± 0.1 eV).

VI. VALENCE-LEVEL SHIFTS FOR Ar/Pd(001), Kr/Pd(001), AND Xe/Pd(001)

The valence levels for different layers in adsorbed rare-gas films also show relative shifts in a way qualitatively similar to the core levels. Figures 8(a), 8(b), and 8(c) show the angle-integrated photoemission spectra for the Xe $5p$,

TABLE IX. Xe $4d$ core-level shifts ΔE_B and Xe NOO Auger-electron energy shifts ΔE_K for a monolayer, bilayer, and trilayer of Xe on Al(111). All energies are in eV. The experimental values of $|\Delta E_K/\Delta E_B|$ are also listed.

Xe/Al(111)	Layer	ΔE_B (expt.)	ΔE_B (theor. 1)	ΔE_K (expt.)	$ \Delta E_K/\Delta E_B $ (expt.)
Monolayer	1	-2.10	-2.69	6.32	3.01
Bilayer	1	-2.22	-2.78	6.50	2.93
	2	-1.67	-1.77	4.66	2.80
Trilayer	1	-2.22	-2.78	6.55	2.95
	2	-1.87	-1.95	5.11	2.82
	3	-1.50	-1.59	4.24	2.83

Kr $4p$, and Ar $3p$ valence levels, respectively, for the indicated layer configurations on Pd(001). These spectra were taken with $h\nu=20$ eV. The spectrum for a Xe monolayer shows, roughly speaking, two peaks: the $5p_{1/2}$ and $5p_{3/2}$; the $5p_{3/2}$ peak shows a structure due to band-dispersion and/or crystal-field-splitting effects. The bilayer spectrum shows two resolved $5p_{1/2}$ peaks associated with the two atomic layers. The multilayer spectrum consists of contributions from all layers, but the signals from the outer few layers dominate. The relative shifts between the outer few layers are small; therefore, the $5p_{1/2}$ peaks are not resolved. The dashed vertical bars in Fig. 8(a) indicate roughly the $5p_{1/2}$ -peak positions for the outermost layer in the three configurations shown. The shifts are qualitatively similar to those of the core levels; the binding energies associated with atoms farther away from the metal substrate are larger due to reduced screening. Similar behaviors are observed for the Kr $4p$ valence levels in Fig. 8(b), but the behavior of the Ar $3p$ valence levels, shown in Fig. 8(c), is less obvious. For example, the bilayer spectrum does not quite resemble a linear combination of contributions from the two layers.

We have tried to deconvolute the spectra for the bi-

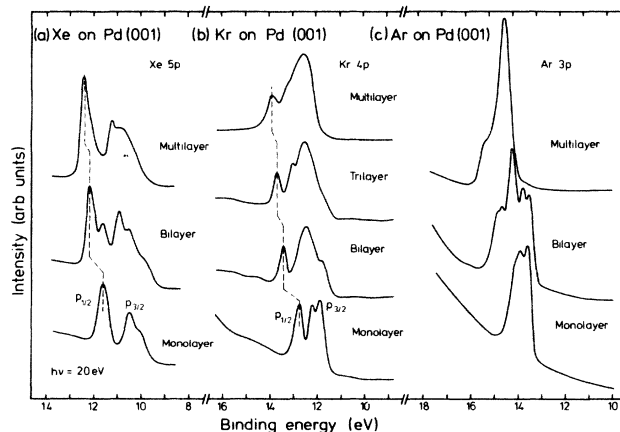


FIG. 8. Angle-integrated valence-level photoemission spectra of monolayers, bilayers, and multilayers of (a) Xe, (b) Kr, and (c) Ar on Pd(001). The Xe $5p_{1/2}$ in (a) and Kr $4p_{1/2}$ in (b), respectively, for the outermost layer, are indicated by the dashed curves.

layers and thicker films for all three rare gases in terms of individual layer contributions, but with very limited success. The quality of the fit is generally not as good as that for the core levels, especially in the case of Ar, indicating non-negligible band-dispersion effects, which would be different for different layers.

A valence excitation in bulk rare-gas solids is not localized; this gives rise to measurable band dispersions. In a thin adsorbed film, the degree of localization of a valence excitation under the influence of the image potential and other effects is not clearly known. Mandel *et al.* determined the layer-by-layer band structure of Xe on Al(111) by measuring the two-dimensional band dispersions for successively thicker layers of Xe.⁸ The results clearly indicate that the valence excitations are delocalized within the atomic plane with measured bandwidths of about 0.5 eV. The bandwidths are actually of the same order of magnitude as the energy shifts between adjacent layers, implying possibly some degree of delocalization also in the direction perpendicular to the substrate surface. Thus, the wave functions associated with the layer-resolved eigenvalues probably have small mixtures from other layers. The simple image-charge formula assuming point-charge configurations cannot be expected to describe the eigenvalue shifts very accurately. The results presented in Fig. 8 indicate that the valence excitations in the Ar film are probably less localized in the direction perpendicular to the substrate surface than in the Kr and Xe films. A more detailed understanding of this subject will undoubtedly involve more theoretical work and angle-resolved measurements of the band structure.

The situation is not any simpler for a monolayer coverage, though the valence excitation has to remain within the atomic plane. For Xe/Pd(001), the measured $|\Delta E_B|$ for Xe $5p_{1/2}$ is about 0.4 eV less than $|\Delta E_B|$ for Xe $4d$.¹ This difference could be due to several effects. Referring to Eqs. (7) and (8), E_s cannot be accurately described by the point-charge image-potential formula because the Xe $5p$ wave function is rather diffuse and the Xe $5p$ excitation is delocalized within the atomic plane. E'_c is expected to be larger than E_c because the valence shell is no longer closed in the final state, leading to possibly a stronger chemisorption-type bond. The $b \Delta W$ term in Eq. (8) may not be entirely negligible as the diffuse Xe $5p$ orbital penetrates somewhat into the surface dipole layer.²⁴

We are unable to estimate reliably the magnitudes of these effects, but we do believe that these effects can explain the 0.4-eV difference in ΔE_B between the core and valence levels.

VII. Ar ON Kr/Pd(001) AND ON Xe/Pd(001)

By adsorbing a submonolayer of Ar on top of a Pd(001) substrate precovered by Kr or Xe layers with various thicknesses, the effect of the metallic substrate screening can be systematically studied without having to deconvolute the spectra, because the Ar levels are well separated from those of Kr and Xe.¹ The angle-integrated photoemission spectra taken with $h\nu=20$ eV for 0.7 monolayer of Ar on Kr-covered Pd(001) and for 0.2 monolayer of Ar on Xe-covered Pd(001) are shown in Figs. 9(a) and 9(b), respectively. The Ar $3p$ features are indicated by the dashed vertical bars in each case; the binding-energy shifts as a function of spacer-layer thickness are evident. On clean Pd(001), the spectrum for 0.7 monolayer of Ar is somewhat different from that for 0.2 monolayer of Ar due to band-dispersion effects. Since the Ar levels are energetically separated from the Kr and Xe levels, the Ar $3p$ holes produced by photoemission are localized within the Ar layer. However, the charge distribution may have a center of gravity slightly displaced from the location of atomic center.

Ar atoms are much smaller than Xe atoms. It is fairly difficult to estimate accurately the adsorption distance for the Ar atoms when they are adsorbed on the Pd(001) substrate or on the Xe (or Kr) films. If a hard-sphere model is used, the on-top sites and hollow sites represent quite different atomic environments. In other words, the substrates can no longer be considered smooth.

Considering the uncertainties mentioned above, we do not present any calculated values of the shifts. We just mention that the measured shifts follow qualitatively the

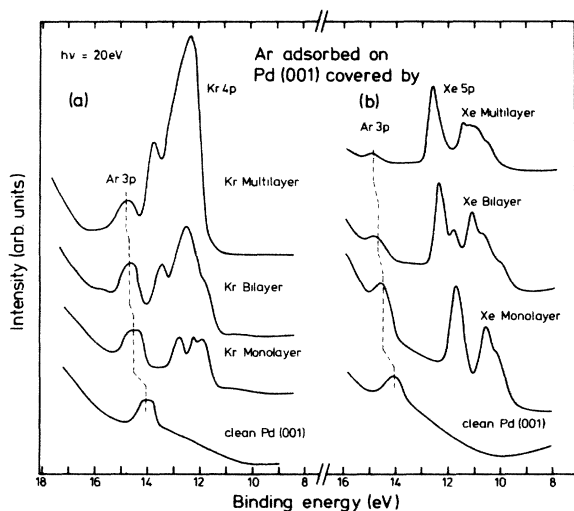


FIG. 9. Angle-integrated valence-level photoemission spectra of (a) 0.7 monolayer of Ar on Kr-covered Pd(001), and (b) 0.2 monolayer of Ar on Xe-covered Pd(001). The Ar $3p$ features as a function of Kr and Xe spacer-layer thickness are indicated by the dashed curves.

trend predicted by the model, and the orders of magnitude of the shifts are also consistent. In a previous study we measured the Xe $4d$ core-level binding-energy shifts and Auger-electron kinetic-energy shifts for a Xe monolayer adsorbed on Pd(001) precovered by Kr. The uncertainties are much less, and the theoretically predicted shifts were indeed in good agreement with the experimental values.¹

VIII. DISCUSSION

The core and Auger shifts can be described quite well by our model. The shifts are dominated by the final-state hole-screening effect. The hole-screening energy is a function of the atomic environment; it increases if there are more nearby rare-gas atoms (dielectric screening) or if the atom is moved closer to a metallic substrate (metallic screening). When a single free Xe atom is adsorbed on a metal surface the core-level binding energies decrease by about 2 eV. If the coverage is increased to a full monolayer, the binding energies decrease further by about 0.2 eV due to screening from nearby Xe atoms.³ The binding energies decrease again slightly if the monolayer is overcoated by another atomic layer of Xe, etc. The core-level binding energies of the second layer are larger than those for the first layer mainly due to reduced metallic screening. These and other general trends are explained well by our model. The theoretical values derived from our simple model with no adjustable parameters also agree well with the experimental values, indicating that the model is quite reasonable.

There are still several points requiring further clarification, to be discussed in the following.

A. Charged versus neutral final state

We mentioned above that recent theoretical and experimental results indicated a fully charged (ionic) photoemission final state for a Xe atom on many metal substrates.^{3,17,18} In the following we will evaluate the Xe $4d$ core-level shift $\Delta E_B(1,1)$ for a Xe monolayer on, say, Al(111), assuming that the final state is neutral. We will see that the theoretical shift is quite different from the experimental value; therefore, our experimental results provide indirect but fairly convincing proof that the photoemission final state is indeed fully charged. A similar argument for the Auger final state will also be given.

Consider the following hypothetical process. We move a Xe adatom Xe(1,1) into the vacuum by providing the energy $E_c(1,1)$. The atom is then photoionized, and Eq. (5) holds. An electron at the Fermi level E_F in the metal substrate is moved into the vacuum and neutralizes the ionized Xe atom by falling into the lowest screening orbital available, the $6s$ orbital of Xe; the net energy required for this step is $W - I^*$, where $W=4.0$ eV is the work function of monolayer-covered Al(111) and I^* is the first ionization energy of the excited neutral Xe atom with the configuration $[\text{Kr}]4d^9 5s^2 5p^6 6s^1$. Using the $Z+1$ or equivalent-core approximation,³¹ I^* is nearly equal to the first ionization energy of a neutral Cs atom, 3.9 eV, with an uncertainty of about ± 0.1 eV.³² This excited neutral Xe atom, Xe^* , is then moved back to its original location on Al(111), releasing a bonding energy $E_c^*(1,1)$ nearly

equal to the bonding energy for a neutral Cs atom. $E_c^*(1,1)$ does not contain the image-charge energy. Following a similar argument leading to Eq. (7), we obtain

$$\Delta E_B(1,1) = E_c(1,1) + W - I^* - E_c^*(1,1). \quad (23)$$

$E_c^*(1,1)$ is larger than $E_c(1,1)$, because a Cs atom binds more strongly to Al(111) than Xe. $E_c(1,1)$, as discussed previously, is about 0.2 to 0.4 eV. We have no experimental value for $E_c^*(1,1)$, but it must be close to the cohesive energy of bulk Cs metal, 0.8 eV.³³ Equation (23) yields $\Delta E_B(1,1) \simeq -0.4$ eV. Even with a very generously estimated error of ± 0.5 eV, the theoretical $\Delta E_B(1,1)$ is still quite different from the experimental value of -2.1 eV. Thus, it seems very unlikely that the final state is neutral.

A related question, which has been discussed much in the literature, concerns the lowest-energy configuration for the final state of photoemission and Auger processes.^{18,34} The lowest-energy configuration is more stable and usually leads to the most prominent sharp structure in the spectrum, provided that the transition matrix element is not small due to negligible wave-function overlap or selection rules. For example, the neutral final state for photoemission (or Auger transition) for Xe on Al(111) involves screening-charge transfer from the substrate, and the associated matrix element may be quite small. The estimated energy difference between the charged and the neutral final-state configurations is easily obtained,¹⁸

$$U^+(4d^9 5s^2 5p^6) - U^*(4d^9 5s^2 5p^6 6s^1) \\ = E_c^*(1,1) + I^* - W - E_c^{++}(1,1), \quad (24)$$

which equals the difference between Eqs. (1) and (23). For Xe on Al(111), Eq. (24) yields $U^+ - U^* = -2.3$ eV, indicating that the charged configuration has a lower energy than the neutral configuration. Since the matrix element leading to the charged final state is expected to be much larger than that leading to the neutral final state, the peaks observed in the photoemission spectra undoubtedly correspond to the charged final state. We did not see any noticeable shake-up features in the spectra, which could be associated with the higher-energy neutral final state. If such shake-up features could be observed and identified, one could determine $U^+ - U^*$ and use Eq. (24) to determine, for example, E_c^* accurately, provided that other quantities on the right-hand side of Eq. (24) are known accurately. One can also use optical-transition data¹⁸ in conjunction with the photoemission data to determine $U^+ - U^*$.

An equation analogous to Eq. (24) can be derived easily for the Auger final state. The energy difference between the doubly ionized state and the singly ionized state is

$$U^{++}(5s^2 5p^4) - U^+(5s^2 5p^4 6s^1) \\ = E_c^{*+}(1,1) + I^{*+} - W - E_c^{++}(1,1), \quad (25)$$

where E_c^{*+} and E_c^{++} are the bonding energies for the singly ionized and doubly ionized states, respectively, and I^{*+} is the first ionization energy of a free Xe ion with the configuration $[\text{Kr}]5s^2 5p^4 6s^1$. Using the $Z + 1$ approximation, I^{*+} is nearly equal to the second ionization energy of a free Ba atom, 10 eV. It is easy to show [see Eqs.

(19)–(21)] that

$$E_c^{*+}(1,1) - E_c^{++}(1,1) \simeq -3E_s(1,1), \quad (26)$$

with an estimated error of about 1 eV. Combining Eqs. (25) and (26), we obtain $U^{++} - U^{*+} = -2.1 \pm 1$ eV. Similarly, the energy difference between the doubly ionized final state and the fully screened neutral final state is

$$U^{++}(5s^2 5p^4) - U^{**}(5s^2 5p^4 6s^2) \\ = E_c^{**}(1,1) + I^{**} + I^{*+} - 2W - E_c^{++}(1,1), \quad (27)$$

where E_c^{**} is the bonding energy for a Xe atom in the fully screened configuration $[\text{Kr}]5s^2 5p^4 6s^2$, and I^{**} is the first ionization energy of a free excited Xe atom with the configuration $[\text{Kr}]5s^2 5p^4 6s^2$. $E_c^{**}(1,1)$ is of the order of the cohesive energy of bulk Ba metal, 1.9 eV.³³ I^{**} is nearly equal to the first ionization energy of a free Ba atom, 5.2 eV.³² Since $E_c^{*+}(1,1) \geq 4E_s(1,1)$ from Eq. (20), we obtain from Eq. (27) that $U^{++} - U^{**} \leq -1.7$ eV, with an estimated uncertainty of ± 1 eV. Thus the doubly ionized final state has the lowest energy. The matrix element also favors heavily the doubly ionized final state because no charge transfer is required. The Auger peaks seen in the photoemission spectra correspond undoubtedly to the doubly ionized final state, and we did not see any clearly identifiable shake-up features in our spectra.

We believe that the same conclusions also apply to Xe on the other two substrates, based on the similarities of behaviors in these three systems.

B. Reference levels

The proper reference level for the adsorbate core-level binding energies has been the subject of considerable discussion.^{10,35} It is really a matter of choice, depending on the particular theoretical model to be used. Experimentally, referring the binding energies to the Fermi level can be done more accurately. We have chosen the vacuum level as the reference because our theoretical model gives directly the binding-energy shifts and Auger-electron kinetic-energy shifts relative to the vacuum level. In other studies, for example, core-level shifts in alloys or surface core-level shifts in metals, it is more convenient to use the Fermi level as the reference.^{36,37}

The reference-level problem is clearly related to the question of the location of the adsorbate core holes relative to the surface dipole layer. This point has been emphasized by Lang *et al.*²⁴ and Gadzuk.³⁵ For Xe adsorbed on jellium, the core levels are *outside* the dipole layer;²⁴ therefore, the vacuum level is a more convenient choice as the reference level.

C. Core-level binding energies of adsorbates nearly independent of substrates

From Tables V, VIII, and IX the Xe $4d_{5/2}$ core-level binding energies for a monolayer coverage on the three substrates Pd(111), Pd(001), and Al(111) are 65.33, 65.23, and 65.45 eV, respectively, referred to the vacuum level. These binding energies are very close to one another. This behavior has been observed in other systems,^{10,12,13,24} and has been explained theoretically by Lang *et al.*²⁴ as a

consequence of the fact that the core levels are outside the surface dipole layer. Within our model, we find that $E_s(1,1)$ is nearly the same for these three substrates and other substrates; therefore, the core-level binding energies should be nearly the same as a result of Eq. (10).

IX. CONCLUSIONS

We have investigated the layer-resolved core-level and Auger-electron kinetic-energy shifts for Xe adsorbed on three different substrates, Pd(111), Pd(001), and Al(111). The behaviors are found to be very similar for these three systems, and the experimental results can be understood using a very simple model. The shifts are dominated by the hole-screening energies, which have been calculated using a jellium model for the metal substrate and using a dielectric continuum model for the rare-gas adlayers. The theoretical values for the shifts obtained without any adjustable parameters are very close to the experimental results, and the small differences are well within the uncertainties of our model. These uncertainties are results of higher-order effects, which cannot be easily calculated.

The general trends of hole-screening energies as a function of the atomic environment can be understood easily. The hole-screening energy increases if there are more nearby rare-gas atoms or if the hole gets closer to the metal substrate. Screening due to the metallic substrate generally leads to larger shifts than screening by nearby rare-gas atoms. Within our model, the Auger kinetic-energy shifts are about minus three times the corresponding core-level binding-energy shifts, and this behavior is observed experimentally.

The model works better when atoms with very similar environments are compared. Thus, the theoretical surface-induced core-level and Auger-electron kinetic-energy shifts relative to the bulk for single-crystal Xe(111) are in very close agreement with the experimental results. The surface-induced shifts are not small in this case, and similar effects must also exist in other systems.

Our model based on a point-charge configuration does not work equally well for valence excitations, which are spatially more extended. More sophisticated theories are necessary for an accurate description of the results. Qualitatively, the valence excitations also show layer-dependent shifts for adsorbed films. Rare-gas atoms adsorbed on metal substrates precoated by different rare-gas films with various thicknesses also show valence-level shifts as a function of the spacer-layer thickness in a manner in qualitative agreement with our model.

By combining results from photoemission, Auger spectroscopy, optical excitations, electron-energy-loss spectroscopy, etc., information about the bonding or cohesive energies of adatoms with different electronic configurations can be deduced. Our results also show that the final states of adsorbed Xe for core-level photoemission and Auger processes are ionic rather than neutral.

ACKNOWLEDGMENTS

This work was supported partially by the U.S. Department of Energy (Division of Material Sciences) under Contract No. DE-AC02-76ER01198 (T.-C.C.), and the Sonderforschungsbereich-6 (TP A1) of the Deutsche Forschungsgemeinschaft (G.K. and T.M.). Two of the authors (T.-C.C. and G.K.) acknowledge the hospitality of and helpful discussions with D. E. Eastman and F. J. Himpsel, IBM Research Center, Yorktown Heights, during the experimental phase of this work, as well as the support by the staff of the Synchrotron Radiation Center of the University of Wisconsin—Madison at Stoughton. The Synchrotron Radiation Center is supported by the U.S. National Science Foundation under Contract No. DMR-80-20164. One of the authors (T.-C.C.) has benefited from discussions with C. P. Flynn of the University of Illinois. We appreciate the comments and suggestions made by G. K. Wertheim of the AT&T Bell Laboratories, who read the manuscript before submission.

¹G. Kaindl, T.-C. Chiang, D. E. Eastman, and F. J. Himpsel, *Phys. Rev. Lett.* **45**, 1808 (1980).

²G. Kaindl, T.-C. Chiang, and D. E. Eastman, *Phys. Rev. B* **25**, 7846 (1982).

³T.-C. Chiang, G. Kaindl, and D. E. Eastman, *Solid State Commun.* **41**, 661 (1982).

⁴G. Kaindl, T.-C. Chiang, and T. Mandel, *Phys. Rev. B* **28**, 3612 (1983).

⁵T.-C. Chiang, G. Kaindl, F. J. Himpsel, and D. E. Eastman, in *Proceedings of the International Conference on X-Ray and Atomic-Inner-Shell Physics, Eugene, 1982*, edited by B. Crasemann (AIP, New York, 1982).

⁶G. Kaindl, T.-C. Chiang, D. E. Eastman, and F. J. Himpsel, in *Ordering in Two Dimensions*, edited by S. K. Sinha (North-Holland, New York, 1980).

⁷K. Horn, M. Scheffler, and A. M. Bradshaw, *Phys. Rev. Lett.* **41**, 822 (1978).

⁸T. Mandel, G. Kaindl, M. Domke, W. Fischer, and W. D. Schneider, *Phys. Rev. Lett.* **55**, 1638 (1985).

⁹T. Mandel, G. Kaindl, K. Horn, M. Iwan, H. U. Middelmann,

and C. Mariani, *Solid State Commun.* **46**, 713 (1983).

¹⁰K. Jacobi and H. H. Rotermund, *Surf. Sci.* **116**, 435 (1982); H. H. Rotermund and K. Jacobi, *ibid.* **126**, 32 (1983).

¹¹R. Opila and R. Gomer, *Surf. Sci.* **127**, 569 (1983).

¹²J. Küppers, H. Michel, F. Nitschke, K. Wandelt, and G. Ertl, *Surf. Sci.* **89**, 361 (1979).

¹³K. Wandelt, J. Hulse, and J. Küppers, *Surf. Sci.* **104**, 212 (1981).

¹⁴B. P. Tonner, *Nucl. Instrum. Methods* **152**, 101 (1978).

¹⁵See, for example, G. K. Wertheim and P. H. Citrin, in *Photoemission in Solids*, edited by K. Cardona and L. Ley (Springer, New York, 1978), Vol. 1, p. 197.

¹⁶L. O. Werme, T. Bergmark, and K. Siegbahn, *Phys. Scr.* **6**, 141 (1972).

¹⁷N. D. Lang, *Phys. Rev. Lett.* **46**, 842 (1981).

¹⁸D. G. Gibbs, J. E. Cunningham, and C. P. Flynn, *Phys. Rev. B* **29**, 5292 (1984); J. E. Cunningham, D. Gibbs, and C. P. Flynn, *ibid.* **29**, 5304 (1984).

¹⁹E. R. Dobbs and G. O. Jones, *Rep. Prog. Phys.* **20**, 516 (1957).

²⁰P. W. Palmberg, *Surf. Sci.* **25**, 598 (1971).

- ²¹P. I. Cohen, J. Unguris, and M. B. Webb, *Surf. Sci.* **58**, 429 (1976).
- ²²M. J. Dresser, T. E. Madey, and J. T. Yates, *Surf. Sci.* **42**, 533 (1974).
- ²³P. A. Redhead, *Vacuum* **12**, 203 (1962).
- ²⁴N. D. Lang and A. R. Williams, *Phys. Rev. B* **25**, 2940 (1982).
- ²⁵N. D. Lang and W. Kohn, *Phys. Rev. B* **7**, 3541 (1973); N. D. Lang and A. R. Williams, *ibid.* **16**, 2408 (1977).
- ²⁶N. Stoner, M. A. van Hove, S. Y. Tong, and M. B. Webb, *Phys. Rev. Lett.* **40**, 243 (1978); M. B. Webb (private communication).
- ²⁷F.-J. Himpsel, N. Schwentner, and E. E. Koch, *Phys. Status Solidi B* **71**, 615 (1975).
- ²⁸B. Sonntag, in *Rare Gas Solids*, edited by M. L. Klein and J. A. Venables (Academic, New York, 1977), Vol. 2, p. 1024.
- ²⁹J. D. Jackson, *Classical Electrodynamics* (Wiley, New York, 1969), p. 111.
- ³⁰A chemisorbed molecule with a strong interaction with the substrate usually has valence-level energies quite different from those in the gas phase. See, for example, T. Gustafsson and E. W. Plummer, in *Photoemission and the Electronic Properties of Surfaces*, edited by B. Feuerbacher, B. Fitton, and R. F. Willis (Wiley, New York, 1978), pp. 353–379.
- ³¹See, for example, C. P. Flynn, *J. Phys. F* **10**, L315 (1980).
- ³²C. F. Moore, *Atomic Energy Levels*, U.S. Natl. Bur. Stand. Circ. No. 467 (U.S. GPO, Washington, D.C., 1971).
- ³³C. Kittel, *Introduction to Solid State Physics*, 3rd ed. (Wiley, New York, 1976), p. 74.
- ³⁴N. D. Lang, A. R. Williams, F. J. Himpsel, B. Reihl, and D. E. Eastman, *Phys. Rev. B* **28**, 1728 (1982).
- ³⁵J. W. Gadzuk, *Phys. Rev. B* **14**, 2267 (1976).
- ³⁶P. Steiner and S. Hüfner, *Solid State Commun.* **37**, 279 (1981).
- ³⁷P. H. Citrin and G. K. Wertheim, *Phys. Rev. B* **27**, 3176 (1983).